Influence of surface channeling in the stopping of protons colliding with LiF surfaces

Andrea J. García and J. E. Miraglia
Instituto de Astronomía y Física del Espacio, Consejo Nacional de Investigaciones Científicas y Técnicas and Departamento de Física, Facultad de Ciencias Exactas y Naturales, Universidad de Buenos Aires, Casilla de Correo 67, Sucursal 28, (C1428EGA) Buenos Aires, Argentina
(Received 3 April 2006; published 21 July 2006)

We investigate the influence the surface description when channeled protons collide grazingly with LiF (100) surfaces in the 100–400 keV energy range. The projectile is considered to move taking into account the (static and dynamic) potentials with all the ions of the grid. In this model the surface reveals not as an impenetrable isotropic plane but as a complicated percolator strongly dependent on the crystallographic indices, and on the initial conditions.

DOI: 10.1103/PhysRevA.74.012902 PACS number(s): 34.50.Bw, 79.20.Rf, 71.10.Ca

I. INTRODUCTION

When a fast heavy projectile impacts on a crystal surface with a grazing angle, it is generally reflected. It happens when the incident angle θ_i is smaller that a certain critical angle θ_c. In its long interacting path (say around 1000 atomic units of distance in our case), the projectile excites target electrons, thus losing energy. The magnitude (electronic) stopping power S describes the total energy lost by the incident ion which can be measured and so it becomes the ultimate validation of the theory used. Excellent reviews on this item were published by Burgdörfer [1], and more recently by Winter [2].

The stopping power is governed by two major aspects of the collision: the projectile trajectory and the differential (local) stopping at every segment of the path. Further, the projectile trajectory depends on the topography of the surface and on the specific interaction potentials with the target ions. All these items will be revisited here.

A first—and well-known—approach to describe the topography of the surface is the so-called *planar* channeling. In this case the surface is considered as a continuous density of atoms or ions. Therefore, the projectile cannot distinguish any texture and it moves rather smoothly. In a second approach, the projectile is allowed to distinguish particular strings of atoms [3]. The so-called *axial* (surface) channeling model considers the surface target formed by strings composed by a continuous (linear) density of atoms along the neighboring crystallographic Miller indices. The incident projectiles along these particular axes can be forced into curved trajectories and thus produce an increment of the stopping power. In this article we go deeper and explore a more realistic description of the surface as composed by ions at the nodes of the crystal. This third approach, that we called *punctual* (surface) channeling, considers the projectile moves colliding with every single point (ions) of the crystal. It can suffer violent collisions at close distances giving rise to more detailed (sinuous) trajectories. In this approach, the topography of the surface is totally surveyed by the incident particle.

The second item that determines the trajectory is the interaction potential. A simple approximation to describe the interaction of the projectile with every single atoms or ions forming the lattice is the Moliere, or Ziegler, Biersack, and Littmark potentials [2]. These potentials are approximations to the Thomas Fermi one expressed in terms of exponential functions. They neglect long-range interactions such as the polarization which is known to play an important role. In this article we will consider not only the best possible Hartree (static) potential but also the dynamic polarization induced by the projectile.

Once we have established the approaches describing the projectile trajectory, i.e., the surface topography and the interacting potentials, all that is left is to tackle the differential stopping at every instant of the path. As the projectile collides with the target nuclei in the punctual channeling, it can suffer violent changes of directions and the usual impact parameter treatment (straight line) is not adequate. We have to resort to an appropriate method to estimate the stopping locally at the differential level. To that end, we have applied the shell-wise local plasma approximation (SLPA) which permits us to evaluate the stopping locally. The SLPA has been successfully used to estimate atomic ionization, stopping in solids, and stopping on surface [4,5]. This approximation requires knowledge of the local electronic density. To describe the electronic density of the ions forming the lattice, we postulate a simple atomic model that we call GII (grid of independent ions). It allows us to use well-known Hartree Fock wave functions.

In synthesis, the basic considerations we assume are the following:

(1) The surface is composed by an array of alkali-metal and halide ions at the places given by the crystal parameters (see Fig. 1).

(2) The electronic wave functions are just the ones of the isolated ions given by the tables of Clementi and Roetti [6] (GII model).

(3) The trajectory of the projectile is calculated classically considering the interaction (static and dynamic polarization) with all the ions of the grid (punctual channeling).

(4) The stopping is calculated assuming successive single atomic collisions accounting at the same time for all the nearest neighborhoods. Quantum interferences among the different centers are neglected [7].

This work deals in particular with collisions of protons on LiF surfaces at high impact energies (larger than 100 keV/u) under punctual channeling considering the individual interaction with all the ions using the SLPA. Atomic units are used unless it is indicated.

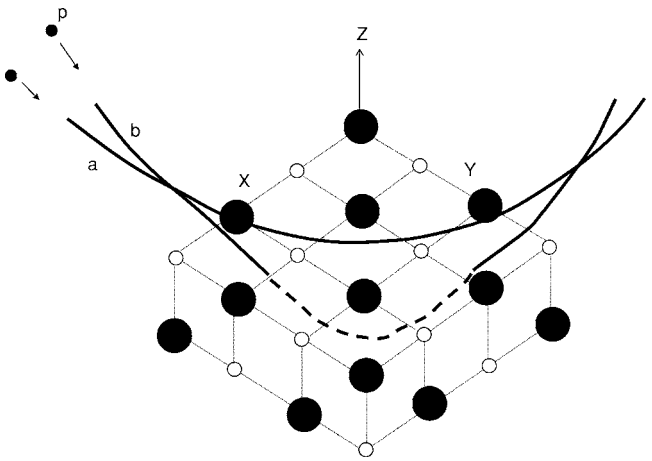

FIG. 1. Schematic diagram.

II. THEORY

A. The differential stopping power

In the case of bare projectiles colliding with a single ion, the stopping probability per unit time in the shellwise local plasma approximation (SLPA) [4,5] reads

$$\frac{dS_{SLPA}(\mathbf{r})}{dt} = \sum_{nl} \int_0^\infty d\omega\, \omega \int_{\omega/v}^\infty dq\, \mathrm{Im}[W_{nl}(q,\omega,\mathbf{r})],$$

$$W_{nl}(q,\omega,\mathbf{r}) = \frac{2Z_P^2}{\pi v}\frac{1}{q}\left[\frac{1}{\varepsilon[q,\omega,k_{Fnl}(\mathbf{r})]} - 1\right], \tag{1}$$

where $k_{Fnl}(\mathbf{r})$ is the space-dependent Fermi velocity, $k_{Fnl}(\mathbf{r}) = [3\pi^2\rho_{nl}(\mathbf{r})]^{1/3}$, $\rho_{nl}(\mathbf{r})$ is the electron density of the nl-state $\rho_{nl}(\mathbf{r}) = |\phi_{nl}(\mathbf{r})|^2$, $\phi_{nl}(\mathbf{r})$ are the bound-state wave functions given in the tables of Ref. [6], and $\varepsilon(q,\omega,k_{Fnl})$ is the Lindhard dielectric function [8]. In Eq. (1), $\mathbf{r}$ is the distance between the projectile and the one ion; the differential stopping involves the sum over all the neighboring ions. The stopping power is then calculated by adding the contributions of the segments of time determined by a Runge Kutta code. The total stopping along a trajectory is

$$S_{SLPA} = \int_{traj.} dt \sum_{s=\pm ijk} \frac{d}{dt} S_{SLPA}(|\mathbf{R}(t) - \mathbf{R}_{ijk}^s|), \tag{2}$$

$\mathbf{R}(t)$ is the projectile coordinate, and $\mathbf{R}_{i,jk}^+$ ($\mathbf{R}_{i,jk}^-$) is the position of the alkalide-metal (halide) ion (Fig. 1). Our SLPA should not be confused with the traditional local plasma (or density) approximation (see, for example, the review of Ziegler [9]); in our case we add shell to shell independently.

B. The ion interaction potentials

We consider two different contributions to describe the interactions of the projectile with the target ions: the *static* (V_{st}) and the *polarization* (V_{pol}) ones.

The static potential is simply the potential created by the ion target considering that the electronic cloud remains frozen. The static potentials, $V_{st}^+(r)$ and $V_{st}^-(r)$ for alkali-metal (Li$^+$) and halide (F$^-$), respectively, can be written as follows:

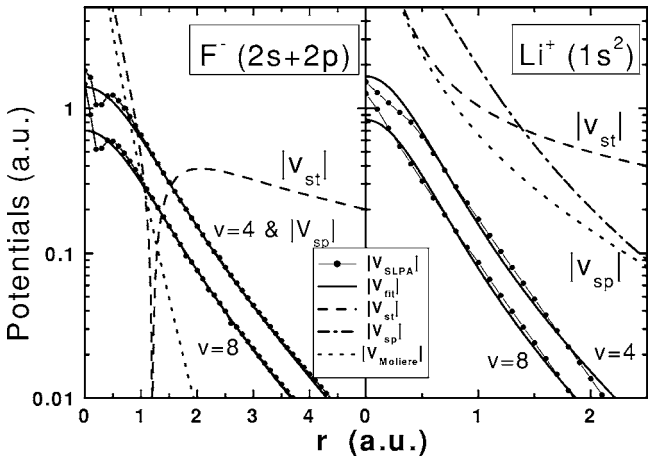

FIG. 2. Absolute values of V_{sp} (dotted-dashed lines), V_{st} (dashed), V_{SLPA} (full circles), and its fitting V_{fit} (solid lines) as a function of the distance to the ions F$^-$ and Li$^+$. The curves displaying V_{SLPA} for $v=4$ and V_{sp} cannot distinguish each other.

$$V_{st}^\pm(r) = \pm\frac{1}{r} + \frac{Z^\pm(r)}{r}, \tag{3}$$

$$Z^+ \to \begin{cases} Z_T^+ - 1, & r \to 0 \\ 0, & r \to \infty \end{cases}, \quad Z^- \to \begin{cases} Z_T^- + 1, & r \to 0 \\ 0, & r \to \infty \end{cases}, \tag{4}$$

where Z_T^+ (Z_T^-) is the target nuclear charge of the alkali-metal (halide). From basic definitions, the Hartree-Fock approximation produces

$$Z^\pm(r) = \sum_{nl} r \int d\mathbf{x} \frac{|\varphi_{nl}^\pm(x)|^2}{|\mathbf{r}-\mathbf{x}|}, \tag{5}$$

where $\varphi_{nl}^\pm$ are, in our case, the Li$^+$ ($1s^2$) and F$^-$ ($1s^2 2s^2 2p^6$) wave functions [6]. To make the calculation tractable, we have fit $Z^\pm(r)$ as a combination of simple exponential functions

$$Z^\pm(r) = \sum_{j=1}^{3} Z_j^\pm \exp(-\mu_j^\pm r). \tag{6}$$

A list of the parameters $Z_j^\pm$ and $\mu_j^\pm$ for Li$^+$ and F$^-$ are shown in Sec. III below. For the fitting procedure we have started with seed values for Z_j and μ_j given by the ones of the Moliere potential. Figure 2 displays the static potentials for F$^-$ and Li$^+$ ions. As it is expected, substantial differences are found at large distances when compared with the Moliere potential.

1. The polarization potential

First, let us start with the *static* polarization potential. It is due to the distortion of the cloud induced by a charge at rest. In its usual form [10,11], it reads

$$V_{sp}^\pm(r) = -\frac{\alpha_0^\pm}{2(r_0^{\pm 2} + r^2)^2}, \tag{7}$$

where $\alpha_0^{\pm}$ is the well-known *static* or electric dipole polarizability and $r_0^{\pm}$ is a cutoff. It is generally related to the radius of the shell; $r_0^2=\langle r^2\rangle$. In general, we define $\langle r^2\rangle=0.75\langle r^2\rangle_{2p}+0.25\langle r^2\rangle_{2s}$. The value of $\alpha_0^{\pm}$ has been calculated with a high degree of precision for most of the neutral atoms and ions. Values for the ions of interest can be found in Refs. [12–14].

For large velocities, we can no longer consider the static term $\alpha_0^{\pm}$ but the *dynamic* polarizability, which depends on the impact velocity v. In accordance with our working model for the stopping [see Eq. (1)], we resort to the self-energy induced by a moving charge in a free electron gas. We introduce the dynamic self-induced potential as

$$V_{SLPA}(r)=-\frac{1}{2\pi v}\sum_{nl}\int_0^{\infty}d\omega\int_{w/v}^{\infty}dq\,\mathrm{Re}[W_{nl}(q,\omega,r)]. \quad (8)$$

In Fig. 2, we plot with full circles $V_{SLPA}(r)$ for Li^+ $(2s^2)$ and F^- $(2s^22p^6)$ for different proton impact velocities. Also in this figure, we show a fitting to V_{SLPA} with a similar expression to Eq. (7) but with $\alpha_{\infty}^{\pm}/v$ instead of $\alpha_0^{\pm}$, i.e.,

$$V_{fit}^{\pm}(r)=-\frac{\alpha_{\infty}^{\pm}/v}{2[r_0^{\pm 2}+r^2+(r/r_6^{\pm})^6]^2}. \quad (9)$$

The dependence of the strength with the inverse of the velocity seems to be very good. At small distances, $V_{SLPA}(r)$ cannot be well fit, but in this case the static potential is dominant and this failure can be overlooked. In fact, the polarization potential drives the collision only for F^- in the range $r\in[1,2]$ where the fitting is quite accurate (see Fig. 2).

The term $(r/r_6^{\pm})^6$ in the denominator of Eq. (9) is included to fit $V_{SLPA}(r)$ at very large distances. In general, we found that r_6 is around 3.6 (2.6) for the halides (alkali-metals). The term $(r/r_6^{\pm})^6$ has been found not to be very relevant in the present calculations and it could be omitted.

At any velocity, we interpolate both extremes (V_{fit} valid for large velocities and V_{sp} valid for $v=0$) by using the following interpolation:

$$V_{pol}^{\pm}(r)=-\frac{\alpha^{\pm}(v)}{2[r_0^{\pm 2}+r^2+\beta^{\pm}(v)(r/r_6^{\pm})^6]^2}, \quad (10)$$

$$\alpha^{\pm}(v)=\frac{\alpha_0^{\pm}}{\sqrt{1+(\alpha_0^{\pm}v/\alpha_{\infty}^{\pm})^2}}\rightarrow\begin{cases}\alpha_0^{\pm} & \text{for } v\rightarrow 0\\ \alpha_{\infty}^{\pm}/v & \text{for } v\rightarrow\infty,\end{cases} \quad (11)$$

$$\beta^{\pm}(v)=\frac{(\alpha_0^{\pm}v)^6}{(\alpha_0^{\pm}v)^6+(\alpha_{\infty}^{\pm})^6}\rightarrow\begin{cases}0 & \text{for } v\rightarrow 0\\ 1 & \text{for } v\rightarrow\infty,\end{cases} \quad (12)$$

which presents the two limits properly.

One observation with respect to the V_{sp} corresponding to Li^+ should be made. Its static polarizability $\alpha_0^{Li+}=8.10$ seems to be unexpectedly large (see Fig. 2); it is as large as the one of F^- $(\alpha_0^{F^-}=10.2)$. This anomaly already has been observed in a previous work [12]. In our case, the dynamic strength of the polarization potential that we use $\alpha^{\pm}(v)$ diminishes its strength substantially. For example, at $v=3$, $\alpha^{Li^+}(v=3)=0.87$ and it makes V_{pol} to be one order of magnitude smaller than V_{sp}.

C. The projectile motion

We can consider the projectile path governed by three different levels of approaches of the surface, namely, planar channeling, surface axial channeling, and the here-called punctual channeling, as explained next.

(i) In the *planar* channeling, the surface is considered as a continuous density of atoms. In this case the potential depends only on the distance to the surface Z and with our potentials, it reads (for each ion)

$$V_{pla}^{\pm}(Z)=\int d\eta[V_{st}^{\pm}(\sqrt{\eta^2+Z^2})+V_{pol}^{\pm}(\sqrt{\eta^2+Z^2})]$$

$$=\sum_j\frac{2\pi Z_j^{\pm}}{\mu_j^{\pm}}\exp(-\mu_j^{\pm}Z)+W_{pol}^{\pm}(Z), \quad (13)$$

$$W_{pol}^{\pm}(Z)\rightarrow-\frac{\pi\alpha^{\pm}(v)}{2(r_0^{\pm 2}+Z^2)}\quad \text{as } r_6\rightarrow\infty. \quad (14)$$

The total potential is simply

$$\mathcal{V}_{spla}(Z)=\sum_{s=\pm,j=0}\delta_{\mathrm{sup}}^s V_{pla}^s\left(Z+j\frac{a}{2}\right), \quad (15)$$

where δ_{sup}^s is the density of positive $(s=+)$ and negative ions $(s=-)$ in the plane. Several planes, $j=1,2,3,\ldots$ one below the other, can be considered separated with a distance $a/2$, a being the lattice parameter. The surface potential depends on the distance to the surface and on the velocity via $\alpha^{\pm}(v)$. The critical angle θ_c is determined in this approach by setting $\mathcal{V}_{spla}(Z=0)=M_P v^2\sin^2\theta_c/2$, M_P being the projectile mass. We found that smaller values of θ_c are obtained when the polarization potential is included.

(ii) In the *surface axial* channeling, the projectile moves in the presence of strings of ions along the projectile direction [3]. The potential depends on the distance to the string ρ. For a given string, the potential reads

$$V_{ax}^{\pm}(\rho)=2\pi\int dl[V_{st}^{\pm}(\sqrt{l^2+\rho^2})+V_{pol}^{\pm}(\sqrt{l^2+\rho^2})]$$

$$=\sum_j\frac{2Z_j^{\pm}}{\rho}K_1(\mu_j^{\pm}\rho)+W_{pol}^{\pm}(\rho), \quad (16)$$

$$W_{pol}^{\pm}(\rho)\rightarrow-\frac{\pi\alpha^{\pm}(v)}{4(r_0^{\pm 2}+\rho^2)^{3/2}}\quad \text{as } r_6-\rightarrow\infty. \quad (17)$$

The total potential is simply

$$\mathcal{V}_{sax}(\rho)=\sum_{s=\pm,l}\delta_l^s V_{ax}^s(\rho+\rho_l), \quad (18)$$

where δ_l^s is the (linear) density of positive $(s=+)$ and negative $(s=-)$ ions in the string characterized by the indices l. The strings to consider depend on the azimuth angle of incidence. We will not consider this case in this article.

(iii) By *punctual* channeling we mean that the projectile moves under the influence of *all* the ions of the crystal grid. In practice, the projectile follows a classical trajectory governed by the Newton equation $\mathbf{F}=M_P d^2\mathbf{R}/dt^2=-\nabla \mathcal{V}_{pun}$, where

$$\mathcal{V}_{pun}(\mathbf{R}) = \sum_{s=\pm i,j,k} V^s(\mathbf{R}-\mathbf{R}^s_{i,jk}), \tag{19}$$

$\mathbf{R}$ is the time-dependent projectile position, $\mathbf{R}^+_{i,jk}$ and $\mathbf{R}^-_{i,jk}$ are again the positions of the ions, alkali-metals, and halides, and $V^{\pm}(\mathbf{R})=V^{\pm}_{st}(\mathbf{R})+V^{\pm}_{pol}(\mathbf{R})$. The indices i, j, and k describes the position of the ions along the axis x, y, and z, respectively. The Newton equations are solved with the initial conditions:

$$\mathbf{R}(0)=\{x_i,y_i,z_i\}, \quad \{x_i,y_i\}\in[0,a], \quad z_i=a, \tag{20}$$

$$\frac{d\mathbf{R}}{dt}(0)=v\{\sin\theta_i\cos\varphi_i,\ \sin\theta_i\sin\varphi_i,\ \cos\theta_i\}. \tag{21}$$

θ_i is the incident polar angle and φ_i is the azimuth angle. The starting position x_i and y_i must be randomized, and z_i should be as large as possible.

III. RESULTS

A. Numerical considerations

The following parameters were obtained: for F^-,

$$\alpha_0=10.93,\ \alpha_\infty=44.0,\ \langle r^2\rangle=1.98,\ r_6=3.6,$$

$$(Z_1,Z_2,Z_3)=(2.063,7.023,0.914),$$

$$(\mu_1,\mu_2,\mu_3)=(1.824,1.834,16.05), \tag{22}$$

and for Li^+,

$$\alpha_0=8.10,\ \alpha_\infty=2.64,\ \langle r^2\rangle=0.445,\ r_6=2.6,$$

$$(Z_1,Z_2,Z_3)=(-0.114,2.492,-0.378),$$

$$(\mu_1,\mu_2,\mu_3)=(1.753,3.711,9.961). \tag{23}$$

As we have mentioned before we use the theoretical value for α_0 for Li^+ given by Refs. [12,14] which is known to be too high. However the values $\alpha(v)$ used are much lower than the static value.

The integration of Eq. (19) has been solved by using a Runge Kutta code with a variable step Δt. At every Δt, we add the stopping produced in this interval, and in this way we solve the integration given by Eq. (2). Thirty-two nearest neighbors were considered, i.e., $4\times4\times2$. This grid is quite convenient because it contains Coulomb-neutral planes as well as any of the axis. The initial distance to the surface was considered to be equal to the crystal parameter, i.e., $z_i=a=7.6$ atomic units. In addition between 10 and 40 values for the couple $\{x_i,y_i\}$ were considered to average the incident projectile initial starting point with respect to the grid. For a given velocity, we have considered 18 incident polar angles θ_i. Per each polar angle we considered 800 equally spaced azimuth angles $\varphi_i\in[0,45°]$ with respect to the index [1,0,0]. The spectrum is symmetric around 45°.

The projectile is reflected from the surface in the direction characterized by θ_f and φ_f which are the outgoing polar and azimuth angles, respectively. As the stopping presents some saw-type oscillations with φ_f, we have smoothed the curves by modulating the results with a Gaussian distribution (as if it were a convolution with an experimental detector) of a width $\Delta=0.1°$, i.e.,

$$S(\theta_f,\varphi_f)=\int_{-\infty}^{+\infty} d\varphi'_f g(\Delta,\varphi_f-\varphi'_f)S(\theta_f,\varphi'_f), \tag{24}$$

$$g(\Delta,\alpha)=\frac{1}{\sqrt{2\pi\Delta^2}}\exp\left[-\frac{1}{2}(\alpha/\Delta)^2\right]. \tag{25}$$

The trajectory is finished when $Z\geq a$ or $Z\leq -a/2$. The projectile rebounds ($\theta_f>0$) when the final position of the projectile reaches values of $Z>a$, and it penetrates the solid ($\theta_f<0$) when $Z<-a/2$. For $v=3$, for example, in a noncritical situation, the collision times are about 700, while in a critical situation it takes up to 3000 or even more. For larger times the proton moves in a very oscillating trajectory, its calculation is very tedious and accumulates numerical errors. We neglect those trajectories where the energy is not conserved within an error of 1%, which means roughly one trajectory in a thousand.

The surface was considered perfectly flat with no terraces or other imperfections. We found interesting cases. For example, a skipping motion, where the projectile ends up trapped in a oscillatory movement due to the attraction of the polarization potential and the subsequent repulsion due to the static potential [15–17]. We also found cases where the proton penetrates the first layers, oscillates inside the solid, and afterwards returns to the vacuum (trajectory b in Fig. 1). These trajectories were found experimentally by Kimura *et al.* [18], and as we shall see they are very relevant in the stopping determination.

B. Results

We have calculated the stopping power and studied the following situations: dependence of the stopping on the polar and azimuth angles, on the rate of penetration, and on the trajectory model.

In Fig. 3 we present the *total* energy loss calculated with the punctual channeling as a function of the incident angle θ_i for three different impact energies $v=2$, 3, and 4 of H^+ on LiF surface. Our model is expected to be valid at large impact velocities, so $v=2$ is not large enough for a reliable validity. We have also plotted the results taking into account solely the topmost atomic plane of ions considering planar (thick solid line) and punctual channeling (open symbols). In the latter case, the number of nearest neighbors considered were $4\times4\times1$. To see the relevance of the second layer, we plot in Fig. 4 the energy spectrum corresponding to the outgoing protons without penetration into the crystal. The spectra shown in the upper figures (one layer) are sharp, while the

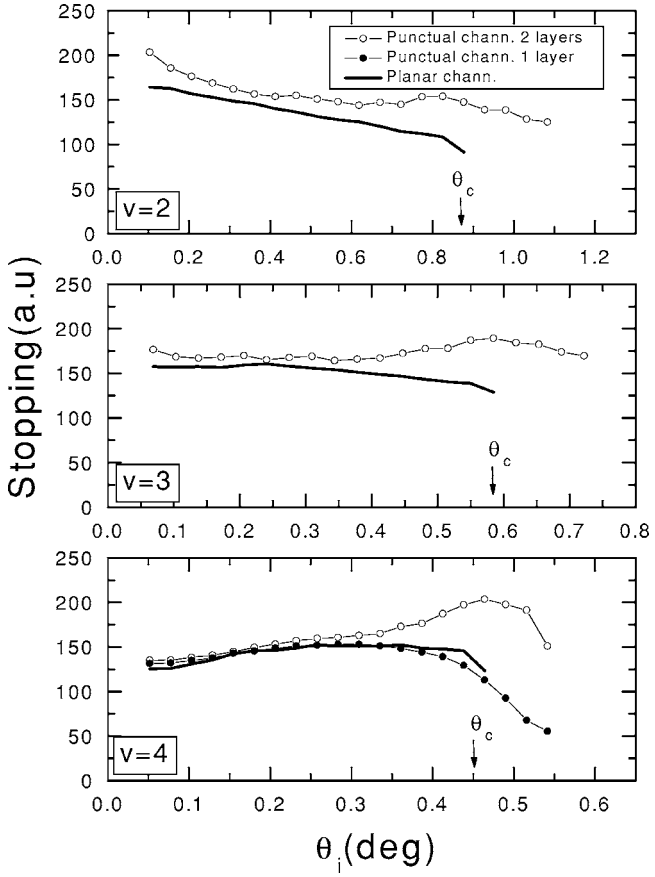

FIG. 3. Stopping power of proton colliding with a LiF(100) surface as a function of the incident polar angle for three incident velocities as it is indicated. Open and solid circles joined with thin solid lines denote the results using the two and one layer punctual channeling, respectively. Thick solid lines denote the results using the planar channeling.

ones in lower figures (two layers) are broader due to the subsurface stopping. This effect becomes relevant as we approach the critical angle.

At small values of θ_i (i.e., $\theta_i \ll \theta_c$), the projectile usually samples the smooth tail of the potentials which is rather well represented by the planar potential (trajectory a in Fig. 1). Around $\theta_i \approx \theta_c$, the one-plane model falls short and the second plane introduces a relevant contribution. The punctual channeling model yields larger stopping than the planar one. Moreover, the two-plane punctual channeling yields larger stopping when compared with the one plane, as is expected. The explanation is simple. At large values of the incident angle θ_i (i.e., $\theta_i \approx \theta_c$), the projectile collides violently with the different ions of the lattice, more oscillating trajectories are observed (larger interaction times) and consequently it produces more stopping. In this range of angles the influence of the second layer below the top is determinant, just as it happens with the penetration phenomena found by Kimura *et al.*, as mentioned before [18].

For a deeper view of this scenario, we plot in Fig. 5 the azimuth dependence for $v=3$ at three angles of incidence. We have integrated on the azimuth angles φ_f as explained before. For this case the critical penetration angle can be calculated in the planar model to give $\theta_c(v=3)=0.58°$. In the planar model the projectile rebounds for $\theta_i < \theta_c$ or penetrates for $\theta_i > \theta_c$. For punctual channeling the situation is much richer. The interesting point here is that even at small θ_i, penetration may occur. It takes place along the more relevant crystallographic axis determined by the indices [100], [110], [210], [310], [510], corresponding to the azimuth angles 0°, 45°, 26°, 18°, and 11°, respectively. Besides these particular axes, the planar channeling gives a very good account of the stopping.

As θ_i increases new crystallographic axes are showed. The surface turns then into a sort of filter. Around the critical angle, $\theta_i \approx \theta_c$, the situation is extremely complicated and the result is strongly dependent on the azimuth φ_i. The planar channeling cannot account for the oscillating trajectories of the projectile and yields smaller stopping. At higher incident angles, $\theta_i > \theta_c$, where the planar channeling forbids the rebound of the projectile, the punctual channeling still allows a reasonable percentage of projectiles to return to the vacuum, as observed in Fig. 6. This figure plots the polar dependence

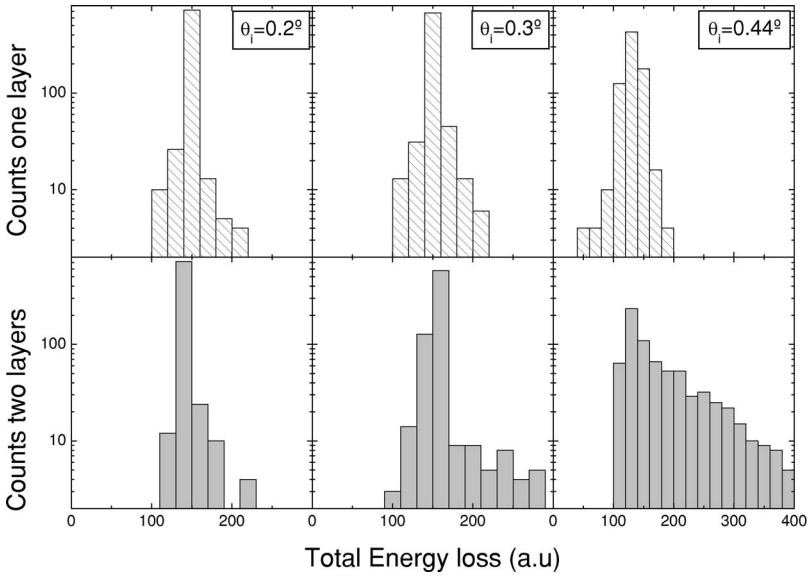

FIG. 4. Energy spectrum of outgoing protons from LiF(100) surface for $v=4$ at three different incident angles, as it is indicated. The spectra shown in the upper figures correspond to one layer and the ones in lower figures to two layers.

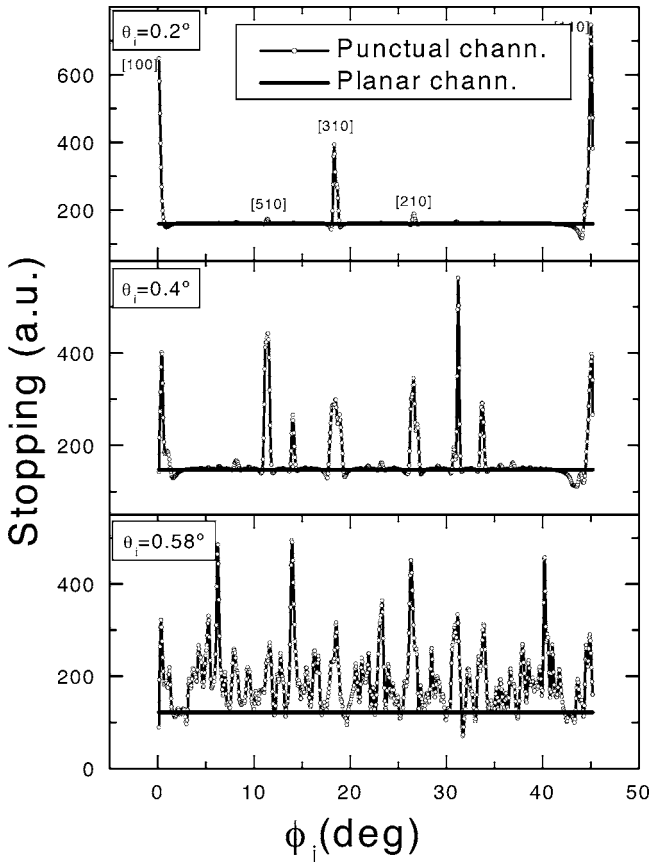

FIG. 5. Stopping power of proton colliding with a LiF(100) surface as a function of the incident azimuth angle for three incident polar angles as it is indicated. The incident proton velocity is 3 (225 keV). Open circles joined with solid lines and thick solid lines denote the results using the punctual and planar channeling models, respectively.

of the penetration (rebound) fraction for impact velocity $v=3$. The punctual channeling predicts about 50% of penetration around $\theta_i \approx \theta_c$, as one would expect.

We have also studied the influence of the polarization potential, which has been generally discarded in most of the previous work. We found that no matter the model, planar or punctual, the polarization potential plays an important role, and it tends in all cases to decrease the stopping substantially. This is simply because the polarization potential attracts the projectile, it accelerates towards the surface diminishing the interaction time. The polarization potential can be seen as provoked by an image charge. This image is constructed by the addition of the induced polarization of all the ions of the target [19]. A relation between the polarization potentials and the self-induced potential is established by the Clausius-Mossotti equation.

IV. SUMMARY

We have calculated the stopping power of ions colliding with insulator surfaces considering that the projectile follows a classical trajectory governed by the interactions with the individual ions of the lattice. To describe the electronic density of the ions forming the lattice, we have postulated a simple atomic model that we call GII (grid of independent ions). Static as well as dynamic polarization potentials were considered. We call this model punctual channeling in contrast with the commonly used planar channeling. Let us summarize our findings:

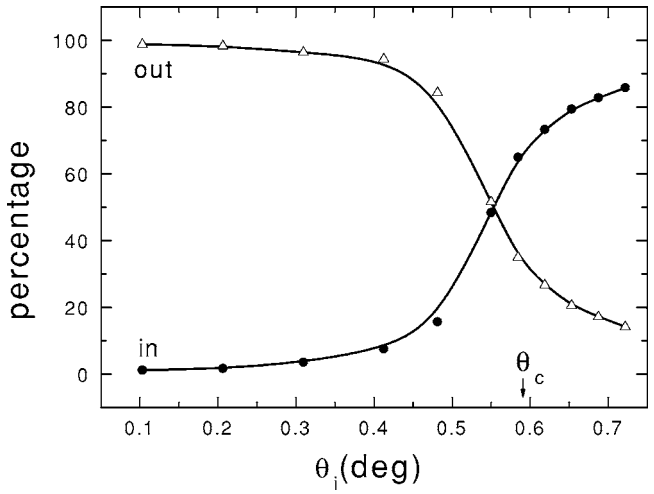

FIG. 6. Reflecting percentage of protons colliding with a LiF (100) surface as function of the incident polar angle for impact velocity 3 (225 keV). The critical angle θ_c is the value calculated with the planar model.

(1) By using the more realistic punctual channeling, we have found the projectiles follow oscillating trajectories, not found in the planar channeling. The surface should not be seen as a impenetrable isotropic plane but as a complicated filter, strongly dependent on the crystallographic indices, and on the initial conditions.

(2) The polarization potential cannot be neglected; it plays an important role. It generally introduces shorter trajectories and significantly reduces the stopping. At this point it is interesting to observe that the advances that we have introduced, punctual channeling and polarization, to some extent compensate (qualitatively) each other. For example, the average stopping calculated with surface channeling discarding the polarization potential yields rather similar values to the punctual channeling calculated with polarization potential.

(3) Around the critical angle of incidence, the influence of the subsurface layers plays a very important role in the stopping. It traps the projectile due to the polarization tail and forces it to oscillate before escaping.

Finally we would like to call attention to the role of the azimuth angle of incidence φ_i when compared with the experimental data. If the experiment is performed at random, the statistics should be done with care: the punctual model predicts very strong oscillations. In our calculations, we needed 800 azimuth angles in the range $[0,45°]$ and the experiments should satisfy at least this same requirement.

ACKNOWLEDGMENTS

This work was done with the financial support of CONICET, UBACyT, and ANPCyT of Argentina.

[1] J. Burgdörfer, in *Review of Fundamental Processes, and Applications of Atoms and Ions*, edited by C. D. Lin (World Scientific, Singapore, 1993) p. 517.
[2] H. Winter, Phys. Rep. **367**, 387 (2002).
[3] G. Andou, K. Nakajima, and K. Kimura, Nucl. Instrum. Methods Phys. Res. B **160**, 16 (2000).
[4] J. E. Miraglia and M. S. Gravielle, Phys. Rev. A **67**, 062901 (2003).
[5] C. C. Montanari and J. E. Miraglia, Phys. Rev. A **73**, 024901 (2006); **73**, 039909(E) (2006).
[6] E. Clementi and C. Roetti, At. Data Nucl. Data Tables **14**, 177 (1974).
[7] M. S. Gravielle and J. E. Miraglia, Phys. Rev. A **71**, 032901 (2005).
[8] J. Lindhard, K. Dan. Vidensk. Selsk. Mat. Fys. Medd. **28**, 8 (1954).
[9] J. F. Ziegler, J. Appl. Phys. **85**, 1249 (1999).
[10] C. J. Joachain, *Quantum Collision Theory* (North Holland, Amsterdam, 1979).
[11] T. M. Miller and B. Bederson, Adv. At. Mol. Phys. **13**, 1 (1977).
[12] N. W. Grimes and R. W. Grimes, J. Phys.: Condens. Matter **10**, 3029 (1998).
[13] D. C. Ghosh and R. Biswas, Int. J. Mol. Sci. **4**, 379 (2003).
[14] R. D. Shannon, J. Appl. Phys. **73**, 348 (1993).
[15] Y. H. Ohtsuki, K. Koyama, and Y. Yamamura, Phys. Rev. B **20**, 5044 (1979).
[16] K. Narumi, Y. Fujii, K. Kimura, Michihiko Mannami, and H. Hara, Surf. Sci. **303**, 187 (1994).
[17] J. Villette, A. G. Borisov, H. Khemliche, A. Momeni, and P. Roncin, Phys. Rev. Lett. **85**, 3137 (2000).
[18] K. Kimura, M. Hasegawa, and M. H. Mannami, Phys. Rev. B **36**, 7 (1987).
[19] H. Winter, Phys. Rev. A **46**, R13 (1992).